RSC Advances

PAPER

View Article Online
View Journal | View Issue

Cite this: *RSC Adv.*, 2023, **13**, 20314

Boosting *o*-xylene removal and power generation in an airlift microbial fuel cell system

Han Chen,[a] Yuanming Li,[b] Zanyun Ying,[c] Yinfeng Xia [a] and Juping You *[d]

Microbial fuel cells (MFCs) are widely acknowledged to be a promising eco-friendly abatement technology of pollutants, and are capable of generating electricity. However, the poor mass transfer and reaction rate in MFCs significantly decrease their treatment capacity for contaminants, especially hydrophobic substances. The present work developed a novel MFC integrated with an airlift (ALR) reactor using a polypyrrole modified anode to promote the bioaccessibility of gaseous *o*-xylene and attachment of microorganisms. The results indicated that the established ALR-MFC system showed excellent elimination capability, with removal efficiency exceeding 84% even at high *o*-xylene concentration (1600 mg m^{-3}). The maximum output voltage of 0.549 V and power density of 13.16 mW m^{-2} obtained by the Monod-type model were approximately twice and sixfold higher than that of a conventional MFC, respectively. According to the microbial community analysis, the superior performances of the ALR-MFC in terms of *o*-xylene removal and power generation were mainly ascribed to the enrichment of degrader (*i.e. Shinella*) and electrochemical active bacteria (*i.e. Proteiniphilum*). Moreover, the electricity generation of the ALR-MFC did not decrease at a high O_2 concentration, as O_2 was conducive to *o*-xylene degradation and electron release. The supplication of an external carbon source such as sodium acetate (NaAc) was conducive to increasing output voltage and coulombic efficiency. The electrochemical analysis revealed that released electrons can be transmitted with the action of NADH dehydrogenase to OmcZ, OmcS, and OmcA outer membrane proteins *via* a direct or indirect pathway, and ended up transferring to the anode directly.

Received 2nd April 2023
Accepted 1st July 2023

DOI: 10.1039/d3ra02174b

rsc.li/rsc-advances

1 Introduction

Microbial fuel cells (MFCs) are an emerging green energy technology that can generate electricity directly during the efficient degradation of contaminants using microbes instead of expensive materials as catalysts.[1] The anode is the fundamental component in MFCs, and its characteristics play a critical role in electron transfer and the redox reaction, and have been the primary reason underlying the low efficiency in various MFC prototypes.[2] The common carbon-based materials, including carbon paper,[3] carbon cloth,[4] carbon felt,[5] graphite felt,[6] graphite brush,[7] and graphite sheet,[8] are widely applied in MFCs owing to their stability and affordability. However, their inherently hydrophobic property is inconducive for microbial adhesion, contributing to poor electron transfer capacity.[2] Many attempts have been made with respect to modification in enhancing MFCs performance and viability. Polypyrrole (PPy) is an attractive polymer used for electrode modification due to its excellent biocompatibility and conductivity. PPy deposition improves the surface roughness and electrical conductivity of the anode, and thus the maximum power density of the MFC was 2.3 times that using unmodified carbon felt.[9]

Besides, substrate mass transfer is another important consideration in the design of reactors, which dominates MFCs performance.[10] Integrated systems are established to improve the insufficient gas–liquid mass transfer of contaminants, especially hydrophobic volatile organic compounds (VOCs). MFC with biological flowing reactor achieved the removal efficiency of ethyl acetate as high as 93.8%.[11] The airlift reactor (ALR) has been extensively utilized in wastewater treatment, air purification, petroleum desulfurization, and other fields due to its exceptional mass and heat transfer rate,[12] ALR was proved to enhance fluid turbulence and accelerate mass transfer rates, obtaining 95.4% *o*-xylene removal efficiency.[13] The removal efficiency and stability of the airlift packing bioreactor was significantly higher than the ALR in removing dichloromethane and toluene, which means that the set of obstacles is profitable in VOCs removal.[14] Moreover, the addition of external carbon source has been confirmed as another effective strategy to enhance system performance. The maximum power density of MFC can be increased from 9.1 to 28.3 W m^{-3} using glucose as an additional substrate.[15] Oxygen content is a vital contributing

[a]*Key Laboratory for Technology in Rural Water Management of Zhejiang Province, Zhejiang University of Water Resources and Electric Power, Hangzhou, 310018, China*
[b]*Zhejiang Zhoushan Tourism and Health College, Zhoushan, 316111, China*
[c]*Ningbo Key Laboratory of Agricultural Germplasm Resources Mining and Environmental Regulation, College of Science & Technology, Ningbo University, Ningbo, 315212, China*
[d]*School of Petrochemical Engineering & Environment, Zhejiang Ocean University, Zhoushan 316022, China. E-mail: youjp@zjou.edu.cn*

parameter for operation capacity of coupled system due to the sensitivity of microorganisms to oxygen,[16] which has not been investigated deeply yet.

In this work, we aimed to develop an ALR-MFC system to overcome the mass transfer limitation in hydrophobic *o*-xylene removal, and the anode modified with PPy was employed to supply more microbial attachment sites and accelerate electron transfer. The system performances including pollutant elimination and electricity generation under different *o*-xylene concentrations were monitored. Also, the effects of oxygen content and external carbon source on reactor operation were evaluated. More detailed, the enhancement mechanism of integrated construction for *o*-xylene degradation was explored based on analysing microbial structure and electrochemical characteristic of the biofilm.

2 Materials and methods

2.1 Reactor setup

The ALR-MFC system was established as shown in Fig. 1. The reactor was made of plexiglass with a diameter of 80 mm and a height of 300 mm, and the working volume of the reactor was 0.9 L. The graphite rod (10 mm in diameter and 250 mm in length) and graphite sleeve modified with PPy (36 mm in inner diameter, 42 mm in outer diameter and 200 mm in length) were used as cathode and anode, respectively. A reference Ag/AgCl (+0.197 V *vs.* standard hydrogen electrode, SHE) was installed to control the anode potential, and all potentials reported here were referred to SHE. In the same electrochemical system, electropolymerization of pyrrole was proceeded through potentiostatic method at 0.9 V in a solution containing 0.1 mol per L PPy, 0.075 mol per L sodium *p*-toluene sulfonic acid, and 0.1 mol per L H_2SO_4 to produce PPy film.[9] Meanwhile, the anode acted as the guide pipe for air lifting. A resistance box (0–9999 Ω) was connected with the ALR-MFC to form a closed circuit. And real time output voltage across the external resistance was gathered by a digital recorder (MIK R5000C; Meacon, Hangzhou, China). The reactor was operated at 30 °C maintained by circulating water through the water jacket.

The inoculum was collected from the long-term running airlift microbial electrolytic cell possessing *o*-xylene removal ability. The electrolyte was composed by phosphate buffer solution (PBS: 2.452 g per L $NaH_2PO_4 \cdot H_2O$, 4.576 g per L Na_2HPO_4, 0.13 g per L KCl, and 0.31 g per L NH_4Cl), 5 mL per L vitamins and 12.5 mL per L trace elements. Vitamin and trace element solutions were prepared as mentioned previously.[13] *O*-xylene (≥99%) and sodium acetate (NaAc, ≥99%) were purchased from Aladdin (Shanghai, China). Other chemicals in this work were of analytic grade supplied by Sinopharm Chemical Reagent Co., Ltd (Shanghai, China). The electrolyte was refreshed every 2–4 day according to its pH variations. The simulated *o*-xylene exhaust gas was synthesized by bubbling the mixed gas of air and N_2 through the bottle containing liquid *o*-xylene, which was further purged into the reactor continuously at total flow rate of 0.6 L min^{-1}. The oxygen content in target pollutant was varied by regulating the flow rates of air and N_2.[1]

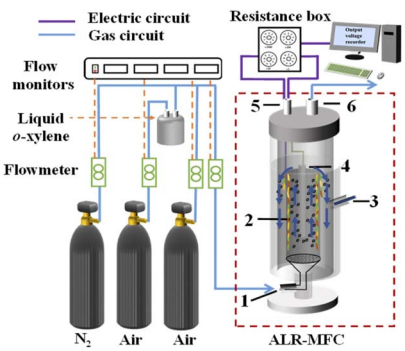

Fig. 1 Schematic diagram of the ALR-MFC system ((1) gas inlet, (2) sleeve-type bioanode, (3) reference electrode, (4) cathode, (5) electric wire interface, (6) gas outlet).

2.2 Experimental procedures

During the start-up phase, *o*-xylene with the concentration of 400 mg m^{-3} was served as the sole carbon source. The empty bed resistance time (EBRT, calculated by divided the volume of the empty ALR-MFC to the inlet gas flow) and external resistance were set at 80 s and 1000 Ω, respectively. In addition, the pH of electrolyte was ranged at 6.8–7.2 during the reactor operation process. The removal efficiency of *o*-xylene was monitored every 12 h until the fluctuation range of removal efficiency was within 5% for 7 d, indicating successful startup of the reactor. In the steady state, the effect of *o*-xylene concentrations ranging from 200 to 1600 mg m^{-3} on pollutant elimination performances including removal, mineralization and coulombic efficiencies as well as power generation capacities including output voltage and power density were evaluated. Moreover, the system performance under different operation conditions such as oxygen concentration (10 and 21%, v/v) and external carbon source (0.5 g per L NaAc) were compared. The electrochemical activity and microbial community structure of biofilm collected from open- and closed-circuit operation modes were analysed to explore the enhancement mechanism of the ALR-MFC reactor for *o*-xylene degradation.

2.3 Analytical methods

The concentrations of *o*-xylene and CO_2 were determined using a gas chromatography (GC9790-II, FULI, China) assembled with a flame ionization detector and thermal conductivity detector, respectively.[4] The gas sampling volume at the inlet and outlet is 0.8 mL and the concentration of *o*-xylene is repeated three times. The removal efficiency, mineralization efficiency, coulombic efficiency, and elimination capacity were calculated according to the eqn (1)–(4), respectively.

$$\text{Removal efficiency } (\%) = \frac{C_{in} - C_{out}}{C_{in}} \times 100\% \quad (1)$$

$$\text{Mineralization efficiency } (\%) = \frac{C_{CO_2}{}' M_{o\text{-xylene}}}{8 \times (C_{in} - C_{out}) M_{CO_2}} \quad (2)$$

$$\text{Coulombic efficiency } (\%) = \frac{M_{o\text{-xylene}} I_{ave}}{FbQ(C_{in} - C_{out})} \quad (3)$$

$$\text{Elimination capacity } \left(\text{g m}^{-3}\ \text{h}^{-1}\right) = \frac{Q(C_{\text{in}} - C_{\text{out}})}{V} \quad (4)$$

where the C_{in} and C_{out} are the inlet and outlet concentrations of *o*-xylene, mg m^{-3}; $C_{CO_2}{}'$ is outlet concentrations of CO_2, mg m^{-3}; $M_{o\text{-xylene}}$ is the relative molecular mass of *o*-xylene; M_{CO_2} is the relative molecular mass of CO_2; I_{ave} is the average current of ALR-MFC system, A; F is the Faraday constant, 96 485 C mol^{-1}; b is the number of electrons transferred; Q is the gas flow rate, $m^3\ h^{-1}$; V is the working volume of the reactor, m^3.

The output voltage and power density, defined as Y, were modelled as a function of *o*-xylene concentration (S) through an empirical Monod-type using the following equation:

$$Y\ \left(\text{V or mW m}^{-2}\right) = \frac{Y_{\max} S}{K_s + S} \quad (5)$$

where $Y_{\max}$ is the maximum voltage or maximum power density, V or mW m^{-2}; S is the *o*-xylene concentration, mg m^{-3}; K_s is the half-saturation constant, mg m^{-3}. And the power density was calculated using the equation:

$$\text{Power density } \left(\text{mW m}^{-2}\right) = \frac{(U_A)^2}{R} \quad (6)$$

where U_A is the output voltage normalized to the projected area of the anode electrode, V m^{-2}; R is the external resistance, Ω.

2.4 Biofilm characterization

The electrochemical characteristic of biofilm were determined by cyclic voltammetry (CV) analysis. CV curves were measured before and after 48 h of operation using the CHI 660E electrochemical workstation (CH Instruments, Inc., Shanghai, China) at a scan rate of 0.001 V s^{-1} over a potential window ranging from −0.6 to +0.6 V in a three-electrode system.[17]

The succession of microbial community was analysed by high-throughput sequencing technology. Microbial DNA was extracted using 3S DNA Isolation Kit V2.2 for environmental samples (Biocolor, Shanghai). The PCR amplification was performed in accordance with the work of Cheng *et al.*[18] PCR reaction process was conducted as follows: 95 °C for 3 min, followed by 30 cycles of 95 °C for 30 s, 55 °C for 30 s, and 72 °C for 30 s, with a final extension step of 72 °C for 5 min. The PCR products were sequenced on the Illumina Miseq desktop sequencer after amplification. More details have been described in our previous work.[19]

3 Results and discussion

3.1 *O*-xylene removal performance of ALR-MFC

The removal efficiency of ALR-MFC maintained at 92% at *o*-xylene concentration lower than 800 mg m^{-3} and then gradually reduced to 84%, while the mineralization efficiency displayed the sustained declining trend as *o*-xylene concentration increased (Fig. 2). A more significant decrease in mineralization efficiency compared to that in removal efficiency at all tested *o*-xylene concentrations was contributed to the recalcitrance of *o*-xylene.[20] Normally, the degradation of *o*-xylene will be terminated before the step of ring-opening. The removal efficiency

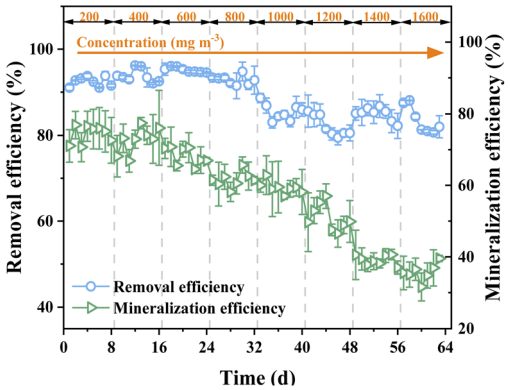

Fig. 2 The effect of *o*-xylene concentration on removal and mineralization efficiencies of ALR-MFC reactor.

and elimination capacity of ALR-MFC were 84% and 57.6 g m^{-3} h^{-1} at *o*-xylene load of 67.7 g m^{-3} h^{-1}, which were 21.7% and 91.9% greater than that of the traditional biological filter obtained at lower pollutant load, respectively.[21] Moreover, the *o*-xylene elimination behaviour of the reactor was also superior, compared to two-chambered MFC whose removal efficiency and elimination capacity were 78% and 4.3 g m^{-3} h^{-1} at 5 g m^{-3} h^{-1} *o*-xylene load,[1] respectively, possibly ascribed to the occurrence of stronger gas–liquid mass transfer in our established system.

3.2 Power generation performance of ALR-MFC

As shown in Fig. 3, the Monod-type model was used to describe the relationship between the power generation performance and the *o*-xylene concentration. The power generation capacity of ALR-MFC displayed a continuous improvement with inlet gas concentration rising from 200 to 1600 mg m^{-3}. It should be noted that the output voltage increased slowly when the inlet *o*-xylene concentration over than 1000 mg m^{-3}. The results of the model fitting (R^2 = 0.997) indicated that the maximum generated voltage was 0.549 V, more than two times higher than that of ordinary MFC reactor.[1] Larger bioanode surface was one of the primary contributors to the greater output voltage. The

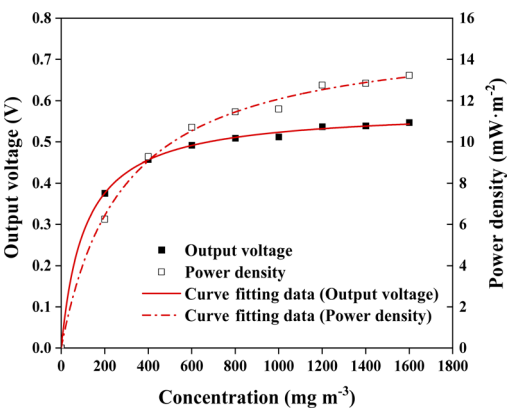

Fig. 3 Monod kinetics modelling of output voltage and power density with respect to *o*-xylene concentration.

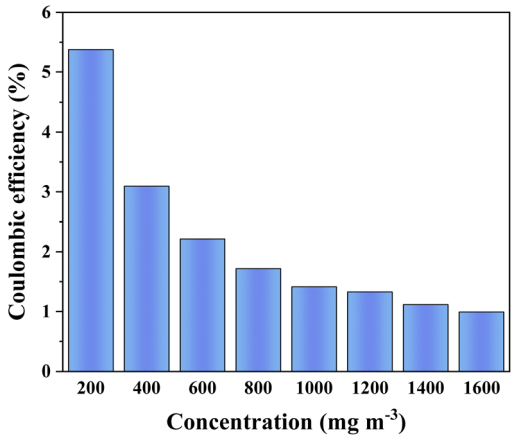

Fig. 4 Effect of *o*-xylene concentration on coulombic efficiency of ALR-MFC.

maximum power density of ALR-MFC achieved as high as 13.16 mW m^{-2}, approximately sixfold better than that of the reported data (2.3 mW m^{-2}).[22] The significant advantages on output voltage and elimination capacity of developed ALR-MFC system demonstrated that the reactor has great potential for efficient conversion from chemical energy of *o*-xylene into electrical energy.

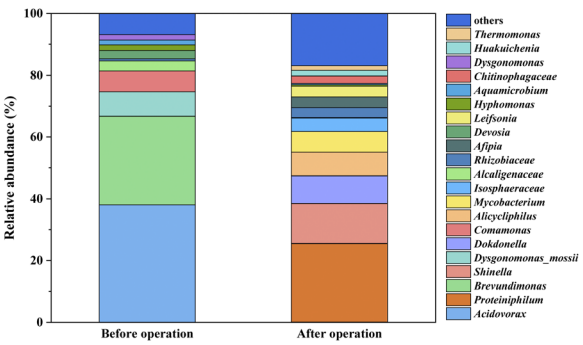

Fig. 5 Microbial community in ALR-MFC reactor in start-up stage and after 150 days operation.

The coulombic efficiency of ALR-MFC in Fig. 4 revealed that the largest coulombic efficiency of 5.37% can be attained at 200 mg m^{-3} *o*-xylene, and then decreased gradually under higher pollution load condition. Although the coulombic efficiency was over twice greater than the MFC feeding with toluene (2.6%),[23] which was poorer than that of MFCs supplied by acetate (coulombic efficiency = 31%),[24] and glucose (coulombic efficiency = 37%).[25] The results emphasized the importance of carbon source types to reactor performance, and the relevant explorations have been conducted in the later section.

3.3 Microbial community in biofilm of ALR-MFC

The succession of microbial community structure before and after operation was shown in Fig. 5. The origin microbial community was mainly consisted of *Acidovorax* (38.05%), *Brevundimonas* (28.6%) and *Dysgonomonas mossii* (7.9%), accounting for 74.55% of the total microbes. The power generation relied on the genus, including *Acidovorax* (Table 1) and *Dysgonomonas mossii*. The dedicated *o*-xylene degraders such as *Brevundimonas* and *Comamonas* also had ability to degrade toluene and *p*-nitrophenol.[26,27] For long-term operation, the relative abundances of *Proteiniphilum*, *Shinella*, and *Dokdonella* increased markedly. Both *Shinella* and *Dokdonella* can degrade toluene and *o*-xylene compounds simultaneously.[28,29] Moreover, previous report has illustrated that *Proteiniphilum* played an essential role in efficient electricity generation.[30] *Alicycliphilus* was in capacity acquiring and consuming electrons,[31,32] lowering the power density.[22] Other bacteria, such as *Leifsonia* and *Mycobacterium* played synergistic roles in *o*-xylene degradation in the bioanode.

3.4 Effect of operating conditions on ALR-MFC performance

3.4.1 Inlet oxygen concentrations. Fig. 6 shows that the oxygen content of *o*-xylene gas has a notable influence on system performance. In Fig. 6a, a decrease of 8.2% in removal efficiency appeared as the oxygen content varied from 21% to 10%, likely due to the activity inhabitation of aerobic predominant degrader such as *Shinella* under low oxygen

Table 1 Main genus of anode biofilm in start-up stage and after 150 days operation[a]

	Proportion (%)				
Genus	Before operation	After operation	Main function	Electron utilization	Ref.
Acidovorax	38.05	<0.3	A & B	Electron consumption	33
Proteiniphilum	<0.3	25.37	A	Electron consumption	30
Brevundimonas	28.60	<0.3	B	—	26
Mycobacterium	<0.3	6.73	B	—	34
Shinella	<0.3	12.96	B	—	29
Dysgonomonas mossii	7.9	<0.3	A	Electron consumption	35
Dokdonella	<0.3	8.87	A & B	Direct electron transfer	28 and 36
Comamonas	6.72	<0.3	A & B	Direct electron transfer	27 and 37
Alicycliphilus	3.12	<0.3	A	Electron consumption	38 and 39
Leifsonia	<0.3	3.45	B	—	40
Dysgonomonas	1.79	<0.3	A & B	Electron consumption	41

[a] A represents the main function of power generation, and B represents the main function of xylene degradation.

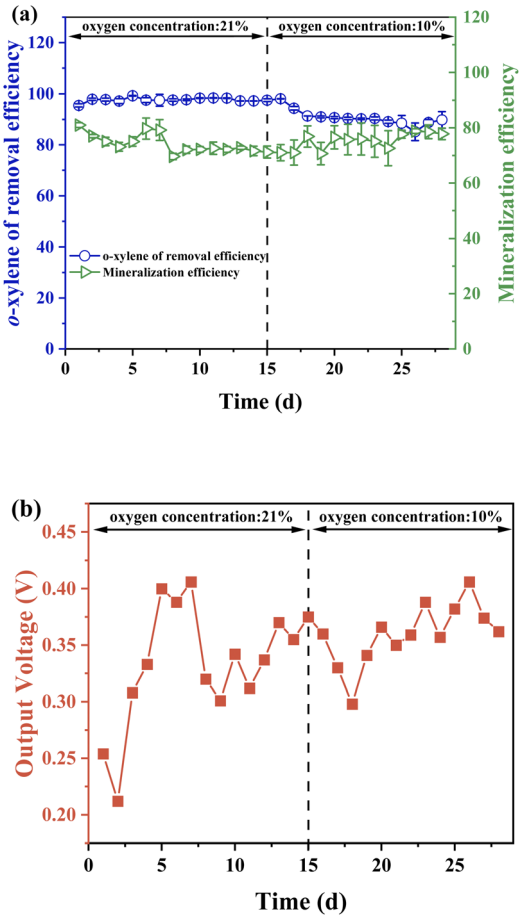

Fig. 6 Effect of oxygen concentration on (a) *o*-xylene removal and mineralization efficiencies, and (b) output voltage of ALR-MFC reactor.

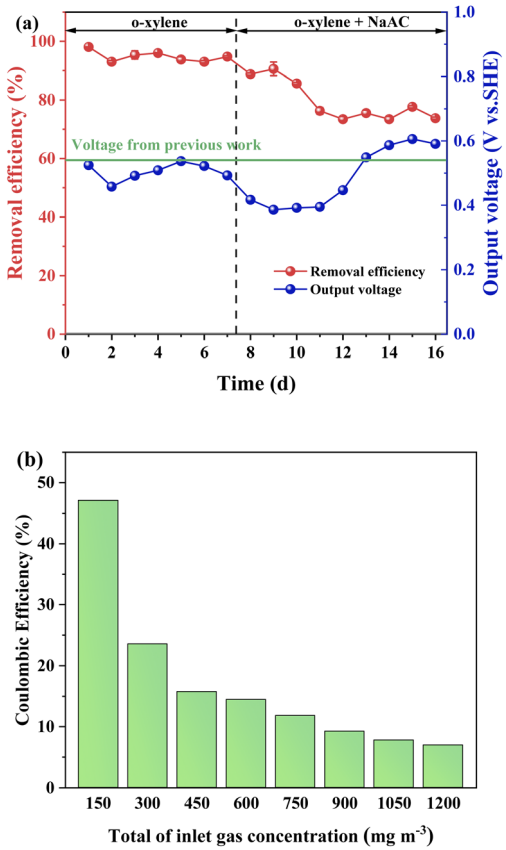

Fig. 7 (a) The removal efficiency and output voltage, and (b) coulombic efficiency of ALR-MFC reactor with 0.5 g per L NaAc addition.

concentration.[42] Differently, an increase of 9.7% in mineralization efficiency emerged with oxygen content decreasing, which was because of the activity promotion for some catabolic enzymes with high oxygen affinities.[43] The output voltages acquired at different oxygen concentrations indicated that generated voltage was not inhibited by a high oxygen concentration (Fig. 6b). Even though the existence of oxygen would induce the competition of electrons with the anode which was supposed to limit output voltage, oxygen could also promote the ring-opening and complete degradation of *o*-xylene to make up the voltage loss caused by oxygen in the mixed gas.

3.4.2 External carbon source. NaAc with the concentration of 0.5 g L^{-1} was added into electrolyte to determine the function of external carbon during *o*-xylene degradation. As presented in Fig. 7a, both the removal efficiency and output voltage dropped after the addition of NaAc, which was caused by the higher bioavailability of NaAc and succession of microbial community. Notably, the output voltage raised to 0.606 V after cultivation for 16 d, exceeding the average voltage reported previously (0.55 V).[44] The improvement in output voltage and decline in removal efficiency suggested that NaAc can enhance the electricity generation performance but not the *o*-xylene elimination capacity of ALR-MFC. Additionally, the coulombic efficiency of system with NaAc shown in Fig. 7b was obviously higher than that of the system without NaAc shown in Fig. 4. The coulombic efficiency was more than 6.9% at all measured *o*-xylene concentrations (150–1200 mg m^{-3}), and the largest coulombic efficiency could reach 47.2%, verifying the enhancement effect of external carbon source on chemical energy to electricity energy.

3.5 Electrochemical characteristic

CV tests were carried out to identify the redox-active components that may be involved in exocellular electron transfer (EET) between biofilm and anode.[45] The CV analyses were measured in the following two conditions, including after replacement of fresh medium and after 48 h of reactor operation. It can be seen from Fig. 8a that there was no significant difference between two CV curves, manifesting that microbial secretions did not participate in the EET process.

The CV curve of anode biofilm was shown in Fig. 8b. The reduction peak at −0.360 to −0.040 V is probably pertained to OmcZ (−0.420 to −0.06 V), OmcS (−0.360 to −0.04 V) and OcmA (−0.350 to −0.08 V).[46] One characteristic oxidation peak at −0.420 to −0.300 V may be corresponded to NAD^+/NADH (−0.477 V).[46] Based on the detected oxidation peaks and its potential corresponding proteins, the electron pathway involved in the *o*-xylene powered ALR-MFC was proposed in Fig. 9. Firstly, *o*-xylene is oxidized to CO_2, H^+ and electrons by anodic

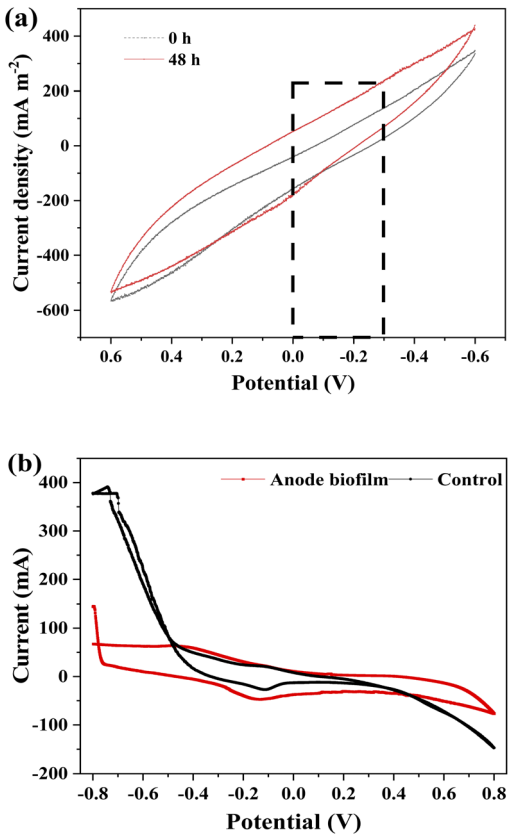

Fig. 8 CV curves of (a) bioanode measured before and after 48 h operation, and (b) anode biofilm.

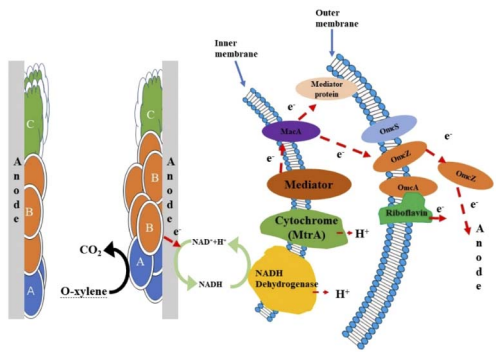

Fig. 9 Proposed electron transfer pathway between biofilm and anode.

attached microorganisms. The released electrons and H^+ could be accepted by intracellular dehydrogenase to produce NADH,[47] which is then transferred H^+ to periplasm and simultaneously transfer electrons to cytochrome. The electrons were then transmitted to outer membrane proteins such as OmcZ, OmcS, and OmcA and finally taken up by anode directly or indirectly.[48]

4 Conclusions

This work established a MFC coupling system with AL reactor for efficient pollutant elimination and power generation. Both the *o*-xylene removal efficiency and the output voltage of the system were enhanced significantly, resulted from the existence of abundant bacteria with capability of degrading *o*-xylene and producing electricity in biofilm. The impacts of operation conditions such as oxygen content and external carbon source on reactor performance were also evaluated. A decrease of 8.2% in *o*-xylene removal efficiency appeared as the oxygen content varied from 21% to 10%, demonstrating the enhancement effect of oxygen for *o*-xylene degradation. Besides, except for the coulombic efficiency improvement, the output voltage achieved as high as 0.606 V with NaAc addition, 10% higher than the reported average voltage (0.55 V). The comparison of CV curves measured before and after running process indicated that electrons can be transferred from biofilm to anode directly *via* inner membrane protein such as NADH dehydrogenase as well as outer membranes proteins such as OmcZ, OmcS, and OmcA.

Author contributions

Han Chen: investigation, writing – original draft, funding acquisition; Yuanming Li: investigation, data curation; Zanyun Ying: investigation, data curation; Yinfeng Xia: validation; Juping You: supervision, writing – review and editing.

Conflicts of interest

There are no conflicts to declare.

Acknowledgements

This research was funded by the "Pioneer" and "Leading Goose" R&D Program of Zhejiang (2022C03146), the National Natural Science Foundation of China (21906151) and the Scientific Research Foundation of Zhejiang University of Water Resources and Electric Power (XKY2022005).

Notes and references

1 J. P. You, Y. Y. Deng, H. Chen, J. X. Ye, S. H. Zhang and J. K. Zhao, *Chemosphere*, 2020, **252**, 126571–126578.
2 Y. Hindatu, M. S. M. Annuar and A. M. Gumel, *Renewable Sustainable Energy Rev.*, 2017, **73**, 236–248.
3 C. Santoro, M. Guilizzoni, J. C. Baena, U. Pasaogullari, A. Casalegno, B. Li, S. Babanova, K. Artyushkova and P. Atanassov, *Carbon*, 2014, **67**, 128–139.
4 X. Q. Lin, L. S. Zheng, M. Zhang, Y. Qin, X. L. Liu, Y. F. Liu, H. Y. Li and C. J. Li, *Chem. Eng. J.*, 2023, **453**, 139910–139917.
5 M. Christwardana, G. E. Timuda, N. Darsono, H. Widodo, K. Kurniawan and D. S. Khaerudini, *J. Power Sources*, 2023, **555**, 232366–232374.
6 M. Kim, S. W. Li, D. S. Kong, Y. E. Song, S.-Y. Park, H. Kim, J. Jae, I. Chung and J. R. Kim, *Chemosphere*, 2023, **313**, 137388–137396.
7 K. Shahid, D. L. Ramasamy, S. Haapasaari, M. Sillanpää and A. Pihlajamäki, *Energy*, 2021, **233**, 121213–121221.
8 Y. Tian, C. Li, D. D. Liang, T. Xie, W. H. He, D. Li and Y. J. Feng, *Sci. Total Environ.*, 2022, **838**, 155926–155935.

9 K. B. Pu, C. X. Lu, K. Zhang, H. Zhang, Q. Y. Chen and Y. H. Wang, *Bioprocess Biosyst. Eng.*, 2020, **43**, 429–437.
10 W. Yang, J. Li, L. Zhang, Z. D. Wei, Q. Liao and X. Zhu, *Renewable Sustainable Energy Rev.*, 2021, **136**, 110460–110474.
11 C. H. Wu, J. C. Shih and C. W. Lin, *Int. J. Hydrogen Energy*, 2016, **41**(47), 21945–21954.
12 J. Behin and P. Amiri, *J. Environ. Manage.*, 2023, **335**, 117560.
13 Y. M. Li, K. Feng, C. Wu, J. Mei, S. H. Zhang, J. X. Ye, J. M. Chen, J. K. Zhao and J. R. Chen, *Chemosphere*, 2021, **291**, 132888–132894.
14 P. L. Xu, Y. Wei, C. H. Ma, S. J. Li, T. J. Guo, X. Q. Wang and W. Li, *J. Environ. Manage.*, 2020, **261**, 109665.
15 H. P. Luo, G. L. Liu, R. D. Zhang and S. Jin, *Chem. Eng. J.*, 2009, **147**(2–3), 259–264.
16 F. Wang, Y. C. Xu, W. Y. Dai, F. Z. Su, J. X. Li, C. S. Zhang, R. Q. Zhang and P. P. Liu, *ACS Sustainable Chem. Eng.*, 2022, **10**, 8559–8567.
17 J. P. You, J. Yu, S. H. Zhang, J. M. Chen and D. Z. Chen, *Chem. Eng. J.*, 2023, **453**, 139731.
18 Z. W. Cheng, K. Feng, D. H. Xu, C. Kennes, J. M. Chen, D. Z. Chen, S. H. Zhang, J. X. Ye and D. D. Dionysiou, *J. Hazard. Mater.*, 2019, **366**, 16–26.
19 W. Li, J. K. Zhao, L. Zhang, Y. F. Xia, N. Liu, S. J. Li and S. H. Zhang, *Sci. Rep.*, 2016, **6**, 18876–18885.
20 N. Gulensoy and P. J. J. Alvarez, *Biodegradation*, 1999, **10**(5), 331–340.
21 S. K. Padhi and S. Gokhale, *Bioresour. Technol.*, 2017, **244**, 270–280.
22 S. H. Zhang, J. P. You, H. Chen, J. X. Ye, Z. W. Cheng and J. M. Chen, *Chem. Eng. J.*, 2020, **386**, 123916–123923.
23 Y. Lang, Y. N. Yu, H. T. Zou, J. X. Ye, S. H. Zhang and J. M. Chen, *Chemosphere*, 2022, **287**, 132247–132253.
24 H. Liu, S. A. Cheng and B. E. Logan, *Environ. Sci. Technol.*, 2005, **39**, 658–662.
25 T. Catal, K. C. Li, H. K. Bermek and H. Liu, *J. Power Sources*, 2008, **175**(1), 196–200.
26 J. G. Huang, Y. Wen, N. Ding, Y. Xu and Q. Zhou, *Bioresour. Technol.*, 2012, **114**, 201–206.
27 H. H. Zhao and C. H. Kong, *Chem. Eng. J.*, 2018, **339**, 424–431.
28 C. M. Fitzgerald, P. Camejo, J. Z. Oshlag and D. R. Noguera, *Water Res.*, 2015, **70**, 38–51.
29 R. Zuo, J. Shi, K. X. Han, D. H. Xu, Q. Li, X. Zhao, Z. K. Xue, Y. X. Xu, Z. Y. Wu and J. F. Wang, *J. Environ. Manage.*, 2022, **317**, 115366–115376.
30 R. Toczyłowska-Mamińska, K. Szymona, P. Król, K. Gliniewicz, K. Pielech-Przybylska, M. Kloch and B. E. Logan, *Energies*, 2018, **11**(1), 124–135.
31 S. A. B. Weelink, N. C. G. Tan, H. ten Broeke, W. van Doesburg, A. A. M. Langenhoff, J. Gerritse and A. J. M. Stams, *FEMS Microbiol. Ecol.*, 2007, **60**, 312–321.
32 J. Hu, L. L. Zhang, J. M. Chen, Y. Luo, B. C. Sun and G. W. Chu, *Chem. Eng. J.*, 2016, **304**, 757–765.
33 L. M. Wang, Q. Q. Pang, Y. Zhou, F. Q. Peng, F. He, W. X. Li, B. Xu, Y. B. Cui and X. Zhu, *Bioresour. Technol.*, 2020, **314**, 123744–123752.
34 L. L. Zhang, C. Zhang, Z. W. Cheng, Y. L. Yao and J. M. Chen, *Chemosphere*, 2013, **90**(4), 1340–1347.
35 X. H. Xie, N. Liu, B. Yang, C. Z. Yu, Q. Y. Zhang, X. L. Zheng, L. Y. Xu, R. Li and J. S. Liu, *Int. Biodeterior. Biodegrad.*, 2016, **111**, 14–21.
36 J. Wang, B. Y. Zhou, R. J. Ge, T. S. Song, J. P. Yu and J. J. Xie, *RSC Adv.*, 2018, **8**, 28613–28624.
37 E. Marsili, J. B. Rollefson, D. B. Baron, R. M. Hozalski and D. R. Bond, *Appl. Environ. Microbiol.*, 2008, **74**(23), 7329–7337.
38 M. J. Oosterkamp, S. Boeren, C. M. Plugge, P. J. Schaap and S. A. J. Stams, *Proteomics*, 2013, **13**(18–19), 2886–2894.
39 V. K. Nguyen, Y. Park, H. Yang, J. Yu and T. Lee, *J. Ind. Microbiol. Biotechnol.*, 2016, **43**(6), 783–793.
40 M. L. Wu, C. Ma, D. Wang, H. Liu, C. C. Zhu and H. N. Xu, *Sci. Total Environ.*, 2020, **713**, 136331–136338.
41 N. Lu, L. Li, C. Z. Wang, Z. R. Wang, Y. Q. Wang, Y. Yan, J. Qu and J. N. Guan, *Sci. Total Environ.*, 2021, **783**, 147045–147055.
42 Y. Huang, Z. Yu, L. Liu, Y. Che and T. Zhang, *Environ. Sci. Technol.*, 2022, **56**, 13097–13106.
43 S. H. Zhang, Z. Y. Ying, J. P. You, J. X. Ye, Z. W. Cheng, D. Z. Chen and J. M. Chen, *RSC Adv.*, 2019, **9**, 15004–15012.
44 R. W. Wang, M. Yan, H. D. Li, L. Zhang, B. Q. Peng, J. Z. Sun, D. Liu and S. Q. Liu, *Adv. Mater.*, 2018, **30**(22), 1800618–1800624.
45 R. M. A. S. Doyle, D. J. Richardson, T. A. Clarke and J. N. Butt, *Electrochim. Acta*, 2013, **110**, 73–78.
46 F. Kracke, I. Vassilev and J. O. Kromer, *Front. Microbiol.*, 2015, **6**, 575–592.
47 N. N. Mordkovich, T. A. Voeikova, L. M. Novikova, I. A. Smirnov, V. K. Il'in, P. E. Soldatov, A. Y. Tyurin-Kuz'min, T. S. Smolenskaya, V. P. Veiko and R. S. Shakulov, *Microbiology*, 2013, **82**(4), 404–409.
48 S. H. Zhang, J. P. You, N. An, J. K. Zhao, L. D. Wang, Z. W. Cheng, J. X. Ye, D. Z. Chen and J. M. Chen, *Chem. Eng. J.*, 2018, **351**, 515–522.